Sound-Based Imaging: Regularization Approaches in Near-field Acoustic Holography

Thomas Martinod Saldarriaga[a]

This manuscript was compiled on May 30, 2024

Regularization of the inverse problem is a complex issue when using Near-field Acoustic Holography (NAH) techniques to identify vibrating sources. This article, aims to compare and implement various regularization methods in the context of NAH. Specifically, it compares the commonly used Tikhonov regularization, sparsity-based regularization and machine learning (ML) regularization for a planar NAH array with measurements obtained from an experimental setup in another study. On another hand, it introduces Green's function-based regularization. The first three types of regularization methods yield images consistent with the results from the referenced study, and statistical indicators are used to determine which method performs best at different frequencies, identifying the behavior of the Tikhonov regularization methods as a lowpass frequency filter.

NAH | Ill posed problems | Regularization

Significance Statement

The significance of this article lies in its exploration and comparison of various regularization methods within the framework of Near-field Acoustic Holography (NAH). By investigating techniques such as Tikhonov regularization, sparsity-based regularization, machine learning (ML) regularization, and Green's function-based regularization, the study provides valuable insights into the efficacy of different approaches for reconstructing normal velocity distributions of vibrating structures. This research addresses the crucial challenge of ill-posed inverse problems encountered in NAH applications, offering potential solutions that can enhance the accuracy and reliability of sound-based imaging techniques. Furthermore, the comparison of these methods against experimental data from a referenced study adds empirical validation to the findings, making this work a significant contribution to the field of sound-based imaging and regularization techniques.

1. Introduction

Nearfield Acoustic Holography (NAH) is a technique widely used for measuring the normal velocity vector and acoustic pressure field of vibrating structures based on close-range sound field measurements. This article focuses on the inverse problem of reconstructing the normal velocity distribution $\dot{w}$ of the source structure, which requires regularization due to ill-conditioning [32].

As on why is this useful, regularization is crucial in various scientific fields, including machine learning and medical imaging. NAH finds industrial applications in acoustic cameras, pipeline leak detection, and emissions measurement [24].

The outline of this article is as follows: first, the development of the continuous and discrete formulation of Nearfield Acoustic Holography (NAH) is initiated, with a focus on solving for the normal velocity field at the source, $\dot{w}$. Following this, several regularization methods are introduced, including Tikhonov, sparsity-based, machine learning (ML), and Green's function. The methodology section elaborates on the origin of the experimental data used to validate the first three regularization methods and provides a brief recap of the algorithms employed. Finally, the results section evaluates the statistical metrics used to measure the accuracy of the regularized images compared to the ground truth images, and presents the best regularized images for the experimental set at four different frequencies.

2. Mathematical Formulation of NAH

A. Continuous Formulation. Two primary approaches exist for developing the mathematical framework essential to understanding nearfield acoustic holography. The first approach relies solely on the acoustic pressure field [20], [21] while the other is centered on the normal velocity scalar field [3], [13]. The mathematical treatment also heavily relies on the geometry of vibrating structures and the corresponding layout of the sensor array [35]. In this study, only planar geometries are considered.

The pressure on a plane at elevation z_0, generated by a plate with a normal velocity distribution $\dot{w}(x, y, 0)$ at elevation 0 and frequency ν (or angular frequency $\omega = 2\pi\nu$), is expressed as the convolution of the source distribution and the propagator $g(\|\vec{r}\|) = g(r) = -i\rho cke^{ikr}/2\pi r$ [33], given by:

$$p(x, y, z_0) = g(x, y, z_0) *_{xy} \dot{w}(w, y, 0) \quad [1]$$

Here, $*_{xy}$ denotes 2-D convolution in the x and y variables, c represents the wave velocity, ρ is the air density, and $k = |\vec{k}| = \omega/c$ denotes the norm of the wavenumber

Author affiliations: [a]Physical Engineering at EAFIT University, Medellín, Colombia

vector. Taking the 2-D spatial transform of equation Eq. (1) with integration variables x and y results in:

$$P(k_x, k_y, z_0) = G(k_x, k_y, z_0)\dot{W}(k_x, k_y, 0) \quad [2]$$

Here, capital letters indicate Fourier 2-D transformed variables, and k_x and k_y represent the wavenumbers in the x and y directions, respectively.

B. Discrete Formulation. The standard approach in Nearfield Acoustic Holography involves a discretized representation of equation Eq. (2), expressed as [30]:

$$\mathbf{p} = \mathbf{F}^{-1}\mathrm{GF}\dot{\mathbf{w}} \quad [3]$$

In this formulation:

- $\dot{\mathbf{w}}$ represents the vector of source normal velocities, discretized on a regularly spaced rectangular grid,
- $\mathbf{p}$ denotes the vector of measured pressures, also discretized within the hologram plane,
- $\mathbf{F}$ denotes the 2-D spatial Discrete Fourier Transform (DFT) operator, and
- $\mathbf{G}$ is predominantly zero except on the diagonal, where it is equivalent to G sampled at the wave vectors of the DFT basis vectors [17].

The matrix product $\mathbf{F}^{-1}\mathbf{GF}$ is denoted as $\mathbf{H}$, with its conjugate transpose represented as $\mathbf{H}^\star$. Solving the inverse problem provides an estimate of the normal velocity $\hat{\dot{w}}$ of the structure. Direct inversion of equation Eq. (3) yields:

$$\hat{\dot{w}} = \mathbf{F}^{-1}\mathbf{G}^{-1}\mathbf{F}\mathbf{p} = \mathbf{H}^{-1}\mathbf{p} \quad [4]$$

Since $\mathbf{G}$ is diagonal and easily invertible, naive inversion of this equation is feasible. However, due to its ill-conditioning, the computation of the sources using this approach is highly unstable, necessitating regularization techniques as described in the subsequent section.

3. Regularization Methods

In this section, the necessity for regularization is elucidated, and the regularization techniques to be employed are introduced.

A. Rationale for Regularization. In the realm of mathematics, a problem is considered well-posed in the Hadamard sense if it satisfies the following criteria:

- The problem possesses a solution.
- The solution is unique.
- Small changes in the initial conditions (data) imply small changes in the response.

Conversely, an ill-posed problem is characterized by the failure of any one of these conditions. In the context of the reconstruction problem posed by Nearfield Acoustic Holography (NAH), two primary reasons render it ill-posed. Firstly, the fundamental theory of planar NAH necessitates the hologram to encompass a larger area than the source, ensuring the inclusion of the limits of the acoustic field produced by the vibrating source. Failure to satisfy this criterion results in field truncation, potentially leading to the non-fulfillment of the existence criterion.

Secondly, based on wave physics principles, the sensor plane, positioned in close proximity to the source plane, is designed to detect both propagating and evanescent waves. The intensity of evanescent waves diminishes exponentially with distance z. Consequently, during back-propagation calculations, measurement uncertainties can induce significant fluctuations in the source field. Since the back-propagation problem in planar NAH is inherently ill-posed, regularization becomes imperative.

B. Tikhonov Regularization. Tikhonov regularization, extensively employed in numerous ill-posed inverse problems, introduces a penalty term to the inverse problem, typically resolving the following minimization problem [9], [11]:

$$\hat{\dot{\mathbf{w}}} = \min_{\dot{\mathbf{w}}} \|\mathbf{p} - \mathbf{H}\dot{\mathbf{w}}\|_2^2 + \lambda\|\mathbf{L}\dot{\mathbf{w}}\|_2^2 \quad [5]$$

Here, $\mathbf{L}$ represents the Tikhonov matrix, and λ denotes the regularization parameter. The outcome of Tikhonov regularization can be obtained in closed form as:

$$\hat{\dot{\mathbf{w}}} = \mathbf{R}_\lambda \mathbf{H}^{-1}\mathbf{p} \quad [6]$$

where $\mathbf{R}_\lambda$ is given by:

$$\mathbf{R}_\lambda = \left(\mathbf{H}^\star\mathbf{H} + \lambda\mathbf{L}^\star\mathbf{L}\right)^{-1}\mathbf{H}^\star\mathbf{H} \quad [7]$$

Two notable points regarding $\mathbf{R}_\lambda$ are:

1. The cancellation of $\mathbf{H}$ and its inverse when equations Eq. (6) and Eq. (7) are merged circumvents the computation of this ill-conditioned inverse.
2. However, it's worth noting that in the fundamental application of Tikhonov regularization to NAH, where $\mathbf{L}$ is chosen as the identity matrix, $\mathbf{R}_\lambda$ functions acts as low-pass spatial filters [3].

C. Sparsity Regularization. Sparsity, a fundamental property of signals, refers to their decomposition as a linear combination of a limited number of pre-defined basis functions, termed atoms. Widely utilized across various domain, sparsity finds applications ranging from data compression to source separation and signal analysis. Formally, a dictionary $\mathcal{D}$, assumed here to have a finite size M, consists of atoms $\mathbf{d}_k \in \mathbb{R}^N : \mathcal{D} = \{\mathbf{d}_k\}_{k=1\dots M}$. $\mathcal{D}$ can either form a basis of $\mathbb{R}^N$ $(M = N)$ or an overcomplete family spanning $\mathbb{R}^N$ $(M > N)$.

A discrete signal $\mathbf{x} \in \mathbb{R}^N$ is deemed sparse in $\mathcal{D}$ if it can be represented as a linear combination of a small subset of atoms [3]:

$$\mathbf{x} = \sum_{j\in J} \alpha_j \mathbf{d}_j \quad [8]$$

where J is a subset of $\{1 \dots M\}$ with $|J| \ll M$. While this decomposition can be exact or approximate, an overcomplete dictionary $\mathcal{D}$ typically lacks a unique representation for a given signal $\mathbf{x}$. To determine the sparsest set of coefficients

α satisfying this equation or achieving the best compromise between data fidelity and sparsity, numerous algorithms, notably ℓ_1 optimization techniques, have been developed.

In the context of NAH, it is assumed that the discretized version of the Fourier-domain velocity map of the source plane $\hat{w}$ is approximately sparse in a suitable basis:

$$\hat{w} \approx \mathbf{D}\boldsymbol{\alpha} \quad [9]$$

Here, the vector $\boldsymbol{\alpha}$ comprises only $|J|$ non-zero elements, and $\mathbf{D} \in \mathbb{R}^{n\times m}$ denotes the matrix whose columns represent all the $\mathbf{d}_k$ in $\mathcal{D}$. Consequently, the NAH inverse problem can be reformulated as follows: given a set of pressure measurements $\mathbf{p}$, find the sparsest set of coefficients α_j such that $\mathbf{p} = \mathbf{HD}\boldsymbol{\alpha}$. Mathematically, this problem can be expressed as:

$$\underset{\alpha}{\operatorname{argmin}} \|\boldsymbol{\alpha}\|_1 \text{ subject to } \mathbf{p} = \mathbf{HD}\boldsymbol{\alpha} \quad [10]$$

It's noteworthy to draw a parallel between Tikhonov regularization Eq. (5) and sparse ℓ_1 regularization. The latter can be represented in Lagrangian form as:

$$\underset{\boldsymbol{\alpha}}{\operatorname{argmin}} \|\mathbf{p} - \mathbf{HD}\boldsymbol{\alpha}\|_2^2 + \lambda\|\boldsymbol{\alpha}\|_1 \quad [11]$$

C.1. Selection of a Dictionary $\mathcal{D}$. Theoretical findings [16] suggest that plane waves offer accurate approximations to solutions of the Helmholtz equation on star-shaped plates, which are characterized by having a point connectable to any other point via a line segment fully contained within the plate. Notably, all convex plates (as rectangular plates) fall under this category. Recent extensions of these results apply to thin isotropic homogeneous plates.

Mathematically, the plate's velocity $\dot{\mathbf{w}}$, as a solution to the Kirchhoff-Love equation, can be approximated by a combination of plane waves and evanescent waves:

$$\dot{\mathbf{w}}(x,y) \approx \left(\sum_n \alpha_n e^{i\vec{k}_n\cdot\vec{r}} + \beta_n e^{\vec{k}_n\cdot\vec{r}}\right)\mathbf{1}_{\mathcal{S}}(x,y) \quad [12]$$

Here, $\mathbf{1}_{\mathcal{S}}(x,y)$ denotes the indicator function that confines the plane waves to the plate's domain $\mathcal{S}$.

D. Machine Learning Regularization. While this method may seem straightforward compared to others discussed here, it's also the most computationally intensive. Mathematically, both previous regularization methods lead to a non-linear optimization problem (Eq. (5), Eq. (11)). An essential question that arises in such problems is how to select the penalization parameter λ?

Since this parameter is unconstrained, one can devise a machine learning iterative algorithm aiming to enhance properties desired by the experimenter. In the context of NAH, where the primary objective is detecting sound sources, contrast becomes paramount for proper source detection. This regularization method leverages either Tikhonov regularization or sparsity regularization, followed by the application of a neural network trained to identify images with heightened contrast. Specifically, it seeks to maximize the absolute difference between a pixel and its Cartesian neighbors.

E. Green's Function Regularization. Let us commence by revisiting the Tikhonov regularization optimization problem:

$$\begin{aligned}\hat{\dot{\mathbf{w}}} &= \underset{\dot{\mathbf{w}}}{\operatorname{argmin}}\, E(\dot{\mathbf{w}}) = \underset{\dot{\mathbf{w}}}{\operatorname{argmin}} \|\mathbf{p} - \mathbf{H}\dot{\mathbf{w}}\|_2^2 + \lambda\|\mathbf{L}\dot{\mathbf{w}}\|_2^2 \\ &= \underset{\dot{\mathbf{w}}}{\operatorname{argmin}} \|\mathbf{H}^{-1}\mathbf{p} - \dot{\mathbf{w}}\|_2^2 + \lambda\|\mathbf{L}\dot{\mathbf{w}}\|_2^2\end{aligned} \quad [13]$$

where $\mathbf{L}$ is the Tikhonov matrix, λ is the regularization parameter, and E is the Tikhonov functional. The concept behind this regularization method is to utilize the functional E that needs to be minimized, and apply the first-order optimality condition $\delta E = 0$ to derive the Euler-Lagrange equations in $\mathbb{R}^3$. Finally, it is derived that [22]:

$$\hat{\dot{\mathbf{w}}}_k(\vec{r}) = \frac{1}{\lambda}\sum_{j=1}^{N}[(\mathbf{H}^{-1}\mathbf{p})_j - \hat{\dot{\mathbf{w}}}(\vec{r}_j)]\, G(\vec{r}_k - \vec{r}_j) \quad [14]$$

which signifies that each component of the normal velocities can be expanded in terms of the columns of the Green's matrix $[G(\vec{r}_k - \vec{r}_j)]_{kj}$. However, the computational implementation of this method proved to be impractical, as it requires prior knowledge of the form of the Green's functions, or iteratively approximating their coefficients in a basis to achieve effective regularization.

4. Methodology

As previously mentioned, this paper focuses purely on mathematical and computational aspects, without conducting any experimental setup. To evaluate the different regularization methods discussed earlier, a reference study with credible and reproducible results is necessary for testing against the proposed methods. The selected reference for conducting the experiments is the article by Chardon and Daudet titled *Nearfield Acoustic Holography using sparsity and compressive sampling principles* [3]. In this study, the authors conducted a physical experiment on a guitar, measuring the discrete acoustic pressure field $\mathbf{p}$ at four different frequencies (ν = 78Hz, 402Hz, 1483Hz, and 3297Hz) to recover the normal velocity field $\dot{w}$. The obtained results were compared with ground truth measurements of the same experiment.

The ground truth measurements were acquired using a laser vibrometer to measure the actual velocity field of the source on a fine regular grid, providing $50 \times 40 = 2000$ vibration impulse responses. For the rectangular plate mentioned, the grid had a 10 mm step along both coordinate axes. The acoustic impulse responses measured by the microphones were processed to provide holograms in the temporal Fourier domain. These holograms, representing harmonic pressure fields, were used for the NAH method. Hologram measurements were performed with an array of 120 electret microphones and a custom-built 128-channel digital recorder. The standard NAH hologram was collected using a 12×10 regular microphone array with a 50 mm square step. The overall dimensions of the array were 550 mm x 450 mm. The array was placed at a distance of $z_0 = 20$

mm from the rectangular plate.

With the data source (the matrix $\mathbf{p}$) identified, the computational analysis conducted in this research is presented step by step:

a) The open-source code (in `MATLAB`) provided by the authors in [3] was accessed and executed, verifying that the results of the code aligned with those reported in the article. Also, databases provided in the same article containing the matrix $\mathbf{p}$ were accessed.

b) For Tikhonov regularization, both the matrix equation Eq. (6) and an optimization solver integrated into the `scipy.optimize` library were employed to solve the nonlinear problem Eq. (5), verifying that they yielded nearly identical results for $\dot{\mathbf{w}}$.

c) For sparsity regularization, the matrix $\mathbf{p}$ was initially expanded into the basis given by Eq. (12) (via direct inner product), ensuring that the majority of coefficients (up to $n = 20$) were zero. Subsequently, the expression Eq. (9) was directly employed to compute the normal velocities in the source plane instead of solving the associated optimization problem.

d) For ML regularization, the nonlinear optimization problem Eq. (11) was solved to prioritize images with higher contrast by selecting λ. To achieve this, a neural network was trained using `pytorch` based on the results obtained in [3].

e) Finally, the magnitude images of the normal velocity field were stored in `.csv` files and plotted using the `matplotlib` library after calculating the statistical indicators that will be presented in the next section.

5. Results

This section presents the statistical indicators used to discern which regularization method produced an image most similar to the ground truth, followed by the selected winning images for each frequency.

A. Statistical Indicators. Four basic statistical indicators were employed for image similarity analysis: C, ε_1, ε_2, and M.

The coefficient of correlation C measures the degree of linear relationship between two images' pixel values. It ranges from -1 to 1, where 1 indicates a perfect positive correlation, and 0 suggests little to no correlation. The correlation coefficient was calculated using the `correlate2d` method from the `scipy.signal` library.

The first-order Root Mean Square Error (RMSE) ε_1 quantifies the average difference between corresponding pixel values of two images. It provides a measure of the overall discrepancy or deviation between the images, with a value of 0 indicating equality. The second-order RMSE ε_2 measures the same but compares the ground truth and the regularized image after applying a first-order blur.

The mean absolute error M is the only dimensional indicator, representing error in units of m/s. While all indicators are crucial and measure the performance of the regularized images, a hierarchical preference is used to select the better image, following the order presented. For the first frequency, $\nu = 78$ Hz, the ground truth image is shown in Figure 1.

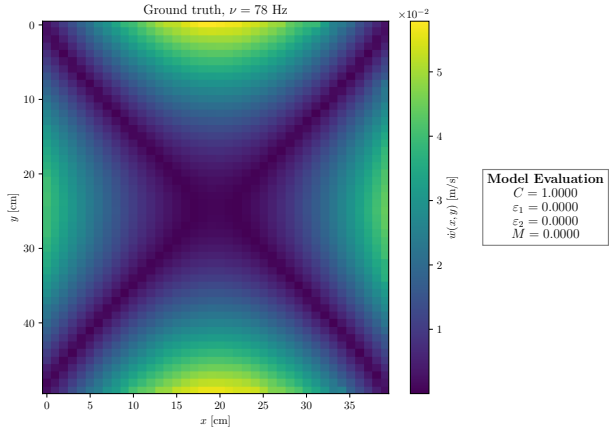

Fig. 1. Ground truth image at $\nu = 78$ Hz.

Among the three regularized images, the one using ML and sparsity regularization yielded the most favorable results. Shown in Figure 2, this method succeeded in identifying sound sources, with a correlation of $C = 0.92$ with the ground truth.

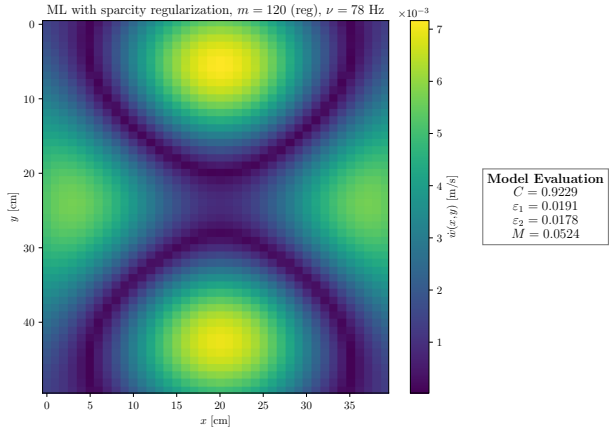

Fig. 2. ML and sparsity regularized image at $\nu = 78$ Hz.

For the mid-range frequency $\nu = 402$ Hz, the closest regularized image to the ground truth was obtained using Tikhonov regularization, with a correlation of $C = 0.94$, as shown in Figure 3.

The results for the frequency $\nu = 1483$ Hz are not presented here. Readers are encouraged to refer to the Appendices and Reproducible Research section, where they can find the images for the methods that were not the closest to the ground truth, along with the ground truth images for each frequency. For this frequency, the closest regularization method was sparsity without ML, suggesting that the original image lacked extreme contrasts, and refining

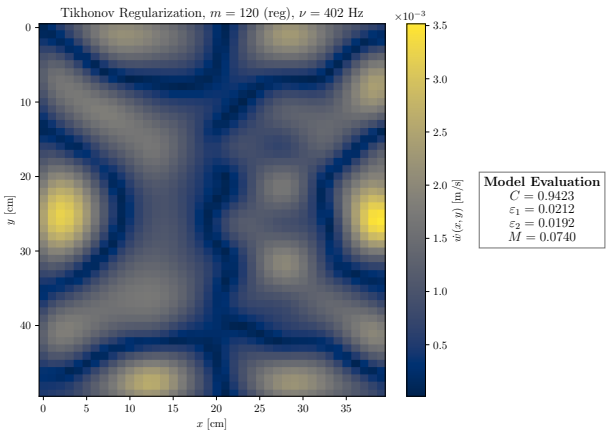

Fig. 3. Tikhonov regularized image at $\nu = 402$ Hz.

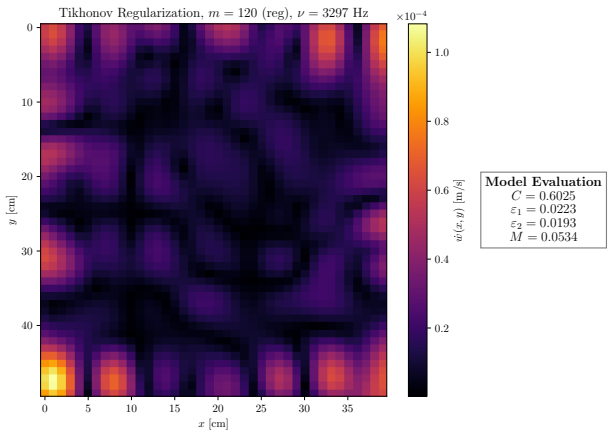

Fig. 5. Tikhonov regularized image at $\nu = 3297$ Hz.

λ based on this criterion induced errors.

Similarly, at the high frequency $\nu = 3297$ Hz, both sparsity without ML and ML regularization methods effectively reproduced the ground truth image. Figure 4 displays the best regularized image, while Tikhonov regularization, as depicted in Figure 5, catastrophically failed due to acting as a lowpass frequency filter in the wavenumber space at higher frequencies [3], [27].

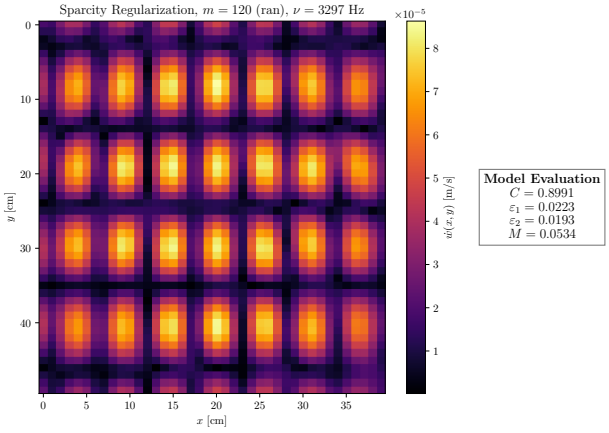

Fig. 4. ML and sparsity regularized image at $\nu = 3297$ Hz.

6. Conclusions

The primary objective of this paper was to evaluate different regularization methods in the context of planar NAH, and this goal was clearly fulfilled. Also, the article presented satisfied the goal of formally describing NAH and all the regularization methods used for creating the images shown, also exhibiting their computational implementation. On another hand, comparisons between the methods were based on strong statistical evidence, and even though no much comment was made on indicators other than C is left to the readers choice his/her preference on which indicator to consider.

The main advance this article represents is that it is one of the first approaches to regularization methods in NAH at a national level, and it serves to encourage further investigation in topics Green's functions regularization.

Finally, as a brief comment on the results section, the order of magnitude of the normal velocities field is not representative of any physical property (unless used for medical purposes). Instead, the constrast (the differences in this normal velocites) is what is used to determine where are the sources located, and it was shown, that goal was achieved.

7. Appendices and reproducible research

All contents, codes, appendices and data used throught this investigation is located at the repository https://github.com/thomas-martinod/proyecto-avanzado-1 under the MIT licence (the contents are mainly in spanish), in alignment with the reproducible research and open science principles [15], [14], [12].

ACKNOWLEDGMENTS. This project would not have been possible without the constant support and technical guidance of my tutor, Professor Nicolás Guarín Zapata from the School of Applied Sciences and Engineering at Universidad EAFIT. Additionally, special thanks go to Professor Elena Montilla Rosero from the same institution for her valuable mentorship. Finally, I extend my heartfelt gratitude to my family, Jules, JuanFer, Fer, and Yoshiro, for their unwavering support.

References

[1] Eugenia Anello. *A Comprehensive Guide of Regularization Techniques in Deep Learning*. Understanding how Regularization can be useful to improve the performance of your model. Dec. 28, 2021. URL: https://towardsdatascience.com/a-comprehensive-guide-of-regularization-techniques-in-deep-learning-c671bb1b2c67 (visited on 02/15/2024).

[2] George Bissinger, Earl G. Williams, and Nicolas Valdivia. "Violin f-hole contribution to far-field radiation via patch near-field acoustical holography". In: *The Journal of the Acoustical Society of America* 121.6 (June 1, 2007), pp. 3899–3906. ISSN: 0001-4966, 1520-8524. DOI: 10.1121/1.2722238. URL: https://pubs.aip.org/jasa/article/121/6/3899/537263/Violin-f-hole-contribution-to-far-field-radiation (visited on 02/14/2024).

[3] Gilles Chardon et al. “Near-field acoustic holography using sparse regularization and compressive sampling principles”. In: *The Journal of the Acoustical Society of America* 132.3 (Sept. 1, 2012), pp. 1521–1534. ISSN: 0001-4966, 1520-8524. DOI: 10.1121/1.4740476. URL: https://pubs.aip.org/jasa/article/132/3/1521/936549/Near-field-acoustic-holography-using-sparse (visited on 02/14/2024).

[4] Tatsuki Fushimi, Kenta Yamamoto, and Yoichi Ochiai. “Acoustic hologram optimisation using automatic differentiation”. In: *Scientific Reports* 11.1 (June 16, 2021). Code repository: https://zenodo.org/records/4906351, p. 12678. ISSN: 2045-2322. DOI: 10.1038/s41598-021-91880-2. URL: https://www.nature.com/articles/s41598-021-91880-2 (visited on 03/02/2024).

[5] Tatsuki Fushimi, Kenta Yamamoto, and Yoichi Ochiai. “Acoustic hologram optimisation using automatic differentiation”. In: *Scientific Reports* 11.1 (June 16, 2021), p. 12678. ISSN: 2045-2322. DOI: 10.1038/s41598-021-91880-2. URL: https://www.nature.com/articles/s41598-021-91880-2 (visited on 03/14/2024).

[6] Parameswaran Hariharan. *Basics of holography*. Cambridge, UK New York, NY: Cambridge University Press, 2002. 161 pp. ISBN: 978-0-521-00200-4 978-0-521-80741-8.

[7] Sabih I. Hayek. “Nearfield Acoustical Holography”. In: *Handbook of Signal Processing in Acoustics*. Ed. by David Havelock, Sonoko Kuwano, and Michael Vorländer. New York, NY: Springer New York, 2008, pp. 1129–1139. ISBN: 978-0-387-77698-9 978-0-387-30441-0. DOI: 10.1007/978-0-387-30441-0_59. URL: http://link.springer.com/10.1007/978-0-387-30441-0_59 (visited on 02/14/2024).

[8] Bernard P. Hildebrand and Byron B. Brenden. *An introduction to acoustical holography*. A Plenum/Rosetta edition. New York: Plenum Publ. Co, 1974. 224 pp. ISBN: 978-0-306-20005-2.

[9] María Josefina Carrió. “Regularización de problemas inversos mal condicionados mediante la minimización de funcionales de tipo Tikhonov-Phillips doblemente generalizados”. MSc. Colombia: Universidad Nacional del Litoral, 2019. 100 pp. URL: https://bibliotecavirtual.unl.edu.ar:8443/bitstream/handle/11185/5466/Tesis.pdf?sequence=1&isAllowed=y (visited on 02/15/2024).

[10] Yang-Hann Kim. “Acoustic Holography”. In: *Springer Handbook of Acoustics*. Ed. by Thomas D. Rossing. New York, NY: Springer New York, 2014, pp. 1115–1137. ISBN: 978-1-4939-0754-0 978-1-4939-0755-7. DOI: 10.1007/978-1-4939-0755-7_26. URL: http://link.springer.com/10.1007/978-1-4939-0755-7_26 (visited on 02/15/2024).

[11] Nguyen Van Kinh. “On the Regularization Method for Solving Ill-Posed Problems with Unbounded Operators”. In: *Open Journal of Optimization* 11.2 (2022), pp. 7–14. ISSN: 2325-7105, 2325-7091. DOI: 10.4236/ojop.2022.112002. URL: https://www.scirp.org/journal/doi.aspx?doi=10.4236/ojop.2022.112002 (visited on 02/14/2024).

[12] Christopher Steven Marcum and Ryan Donohue. *Breakthroughs for All: Delivering Equitable Access to America’s Research*. OSTP blog. Aug. 25, 2022. URL: https://www.whitehouse.gov/ostp/news-updates/2022/08/25/breakthroughs-for-alldelivering-equitable-access-to-americas-research/ (visited on 02/15/2024).

[13] J. D. Maynard, E. G. Williams, and Y. Lee. “Nearfield acoustic holography: I. Theory of generalized holography and the development of NAH”. In: *The Journal of the Acoustical Society of America* 78.4 (Oct. 1, 1985), pp. 1395–1413. ISSN: 0001-4966, 1520-8524. DOI: 10.1121/1.392911. URL: https://pubs.aip.org/jasa/article/78/4/1395/779266/Nearfield-acoustic-holography-I-Theory-of (visited on 02/14/2024).

[14] MINISTERIO DE CIENCIA TECNOLOGÍA E INNOVACIÓN – MINCIENCIAS. *Política Nacional de Ciencia Abierta*. May 27, 2022. URL: https://minciencias.gov.co/sites/default/files/ckeditor_files/Documento%20consulta%20p%C3%BAblica%20-%20Pol%C3%ADtica%20Nacional%20de%20Ciencia%20Abierta.pdf (visited on 02/15/2024).

[15] MINISTERIO DE CIENCIA, TECNOLOGÍA E INNOVACIÓN. *Política Pública de Apropiación Social del Conocimiento en el marco de la CTeI*. Mar. 2021. URL: https://minciencias.gov.co/sites/default/files/politica_publica_de_apropiacion_social_del_conocimiento.pdf (visited on 02/15/2024).

[16] A. Moiola, R. Hiptmair, and I. Perugia. “Plane wave approximation of homogeneous Helmholtz solutions”. In: *Zeitschrift für angewandte Mathematik und Physik* 62.5 (Oct. 2011), pp. 809–837. ISSN: 0044-2275, 1420-9039. DOI: 10.1007/s00033-011-0147-y. URL: http://link.springer.com/10.1007/s00033-011-0147-y (visited on 05/29/2024).

[17] R. K. Mueller and N. K. Sheridon. “Sound Holograms and Optical Reconstruction”. In: *Applied Physics Letters* 9.9 (Nov. 1, 1966), pp. 328–329. ISSN: 0003-6951. DOI: 10.1063/1.1754771. URL: https://doi.org/10.1063/1.1754771 (visited on 03/10/2024).

[18] Jia-cheng Ni et al. “L1/2 Regularization Sar Imaging Via Complex Image Data: Regularization Parameter Selection for Target Detection Task”. In: *IGARSS 2018 - 2018 IEEE International Geoscience and Remote Sensing Symposium*. IGARSS 2018 - 2018 IEEE International Geoscience and Remote Sensing Symposium. Valencia: IEEE, July 2018, pp. 2298–2301. ISBN: 978-1-5386-7150-4. DOI: 10.1109/IGARSS.2018.8519138. URL: https://ieeexplore.ieee.org/document/8519138/ (visited on 02/14/2024).

[19] Luis Rincón. *Curso Intermedio de Probabilidad*. Ciudad de México: Facultad de Ciencias UNAM, Oct. 2007. URL: http://personal.cimat.mx:8181/~pabreu/LuisRincon.pdf.

[20] R. (Rick) Scholte. “Fourier based high-resolution near-field sound imaging”. In: (2008). In collab. with Roozen NB (Bert), Nijmeijer H (Henk), and Lopez I (Ines). Publisher: [object Object]. DOI: 10.6100/IR639528. URL: https://research.tue.nl/en/publications/fourier-based-highresolution-nearfield-sound-imaging(1bd464b0-e91c-4573-bb81-6a72fa0c289d).html (visited on 03/14/2024).

[21] Rick Scholte. *Fourier Based Near Field Acoustic Holography*. Eindhoven University of Technology, Mar. 31, 2015. URL: https://www.youtube.com/watch?v=AEJSE_GKozE&ab_channel=Sorama.

[22] S Sengupta. *Lec-27 Solution of Regularization Equation: Greens Function*. URL: https://www.youtube.com/watch?v=4U3P0LcaJcw&ab_channel=nptelhrd (visited on 05/29/2021).

[23] Howard M. Smith. *Principles of holography*. New York: Wiley-Interscience, 1969. 239 pp. ISBN: 978-0-471-08340-5.

[24] Sorama. *Sorama - Make sound insightful*. https://sorama.eu/.

[25] Steve Mould. *Acoustic cameras can SEE sound*. Mar. 20, 2023. URL: https://www.youtube.com/watch?v=QtMTvsi-4Hw (visited on 03/02/2024).

[26] Albert Tarantola. *Inverse Problem Theory and Methods for Model Parameter Estimation*. Society for Industrial and Applied Mathematics, Jan. 2005. ISBN: 978-0-89871-572-9 978-0-89871-792-1. DOI: 10.1137/1.9780898717921. URL: http://epubs.siam.org/doi/book/10.1137/1.9780898717921 (visited on 02/15/2024).

[27] A. N. Tikhonov and V. IA Arsenin. *Solutions of ill-posed problems*. Scripta series in mathematics. Washington : New York: Winston ; distributed solely by Halsted Press, 1977. 258 pp. ISBN: 978-0-470-99124-4.

[28] Nicolas P. Valdivia. “Krylov Subspace iterative methods for time domain boundary element method based nearfield acoustical holography”. In: *Journal of Sound and Vibration* 484 (Oct. 2020), p. 115498. ISSN: 0022460X. DOI: 10.1016/j.jsv.2020.115498. URL: https://linkinghub.elsevier.com/retrieve/pii/S0022460X20303308 (visited on 02/15/2024).

[29] David Lee Van Rooy. “Digital Ultrasonic Wavefront Reconstruction in the Near Field”. Texto. Rice University, 1971. 81 pp. URL: https://repository.rice.edu/items/dbeb39f7-30af-4df1-8ffb-67c148615054 (visited on 02/13/2024).

[30] W. A. Veronesi and J. D. Maynard. “Nearfield acoustic holography (NAH) II. Holographic reconstruction algorithms and computer implementation”. In: *The Journal of the Acoustical Society of America* 81.5 (May 1, 1987), pp. 1307–1322. ISSN: 0001-4966. DOI: 10.1121/1.394536. URL: https://doi.org/10.1121/1.394536 (visited on 03/10/2024).

[31] Wikipedia. *Holography*. URL: https://en.wikipedia.org/wiki/Holography.

[32] Earl G. Williams, J. D. Maynard, and Eugen Skudrzyk. “Sound source reconstructions using a microphone array”. In: *The Journal of the Acoustical Society of America* 68.1 (July 1, 1980), pp. 340–344. ISSN: 0001-4966, 1520-8524. DOI: 10.1121/1.384602. URL: https://pubs.aip.org/jasa/article/68/1/340/773621/Sound-source-reconstructions-using-a-microphone (visited on 02/14/2024).

[33] Earl George Williams. *Fourier acoustics: sound radiation and nearfield acoustical holography*. San Diego, Calif: Academic Press, 1999. ISBN: 978-0-12-753960-7.

[34] Qing Wu, Tianlu Ma, and Fan Wang. “Modified Lanczos Algorithm for L2,1 norm Regularization Extreme Learning Machine”. In: *2021 International Conference on Control, Automation and Information Sciences (ICCAIS)*. 2021 International Conference on Control, Automation and Information Sciences (ICCAIS). Xi’an, China: IEEE, Oct. 14, 2021, pp. 679–684. ISBN: 978-1-66544-029-5. DOI: 10.1109/ICCAIS52680.2021.9624517. URL: https://ieeexplore.ieee.org/document/9624517/ (visited on 02/15/2024).

[35] Xuxin Zhang et al. “Statistically Optimized Near-Field Acoustic Holography Using Prolate Spheroidal Wave Functions”. In: *Shock and Vibration* 2023 (Aug. 31, 2023). Ed. by Arcanjo Lenzi, pp. 1–20. ISSN: 1875-9203, 1070-9622. DOI: 10.1155/2023/9954054. URL: https://www.hindawi.com/journals/sv/2023/9954054/ (visited on 02/15/2024).